ELSEVIER

Polymer 42 (2001) 9121–9131

polymer

www.elsevier.com/locate/polymer

Hard and soft confinement effects on polymer crystallization in microphase separated cylinder-forming PEO-*b*-PS/PS blends

Lei Zhu[a], Brion R. Mimnaugh[a], Qing Ge[a], Roderic P. Quirk[a], Stephen Z.D. Cheng[a,*], Edwin L. Thomas[b], Bernard Lotz[c], Benjamin S. Hsiao[d], Fengji Yeh[d], Lizhi Liu[d]

[a]*Department of Polymer Science, Maurice Morton Institute, The University of Akron, 170 University Circle, Akron, OH 44325-3909, USA*
[b]*Department of Materials Science and Engineering, Massachusetts Institute and Technology, Cambridge, MA 02139, USA*
[c]*Institute Charles Sadron, 6 Rue Boussingault, Strasbourg 67083, France*
[d]*Department of Chemistry, The State University of New York at Stony Brook, Stony Brook, NY 11794-3400, USA*

In the occasion of Professor Richard Stein's 75th birthday for his life-time contributions in polymer science and engineering

Received 8 March 2001; accepted 13 April 2001

Abstract

A lamellae-forming poly(ethylene oxide)-*b*-polystyrene (EOS) has been blended with a polystyrene homopolymer (PS) and a PS oligomer (PSO), respectively, to obtain miscible polymer blends (denoted as EOS/PS-32 and EOS/PSO-32, respectively). Both blends exhibit cylindrical microphase morphologies, with the PEO volume fractions being 0.32. The order–disorder transition temperatures (T_{ODT}) of both blends are 175 and 84°C, respectively, as determined by temperature-dependent small angle X-ray scattering experiments. The glass transition temperature of the PS matrix (T_g^{PS}) for the EOS/PS-32 blend is 64°C as determined by differential scanning calorimetry (DSC), while that for the EOS/PSO-32 blend is only 16°C. Thus, by controlling the crystallization temperatures (T_c^{PEO}), two kinds of nano-confined PEO crystallizations have been achieved in these blends: when $T_{ODT} \gg T_g^{PS} > T_c^{PEO}$ in the EOS/PS-32 blend, the PEO-block crystallization is confined under a *hard* PS confinement, while for $T_{ODT} > T_c^{PEO} \gtrsim T_g^{PS}$ in the EOS/PSO-32 blend, the PEO-block crystallization is confined under a *soft* PS confinement. DSC and wide-angle X-ray experiments show that the crystallizations of the PEO blocks in these two confinement environments behave differently. The PEO-block crystallization kinetics in the hard confinement is much slower than that in the soft confinement. The DSC kinetics studies show that for $T_c < 30$°C, the $\ln K$ values in the Avrami equation for both blends appear similar, while the n parameter for the EOS/PSO-32 is higher than that for the EOS/PS-32 blend. The melting temperature and weight percent crystallinity of the PEO crystals in the soft confinement environment are higher than those in the hard confinement environment, indicating that the PEO crystals developed in the soft confinement environment possess higher thermodynamic stability than in the hard confinement environment. Furthermore, heating the PEO crystals in the soft confinement environment can continuously increase their thermodynamic stability through a crystal thickening process, by which the soft confinement environment is partially destroyed. © 2001 Published by Elsevier Science Ltd.

Keywords: Crystalline–amorphous diblock copolymer; AB/A polymer blend; Microphase separation

1. Introduction

Recently, confined polymer crystallization has received substantial attention. A simple and effective way to study nano-confined polymer crystallization is to use crystalline–amorphous diblock copolymers as templates. The confinement geometries include: lamellae [1–11], cylinders [4,7,11–15], and spheres [16–18]. Generally, three competing physical events determine the final phase and crystalline morphologies of a crystalline–amorphous diblock copolymer, i.e. the microphase separation of the diblock copolymer, the crystallization of the crystallizable blocks, and the vitrification of the amorphous blocks. Accordingly, three temperature parameters associated with these physical events are of great importance, namely, the order–disorder transition temperature of the diblock copolymer (T_{ODT}), the crystallization temperature of the crystallizable blocks (T_c^c), and the glass transition temperature of the amorphous blocks (T_g^a) [19].

Both unconfined and confined crystallization have been observed in crystalline–amorphous diblock copolymers. For the unconfined crystallization, the crystallization interaction overwhelms the microphase separation. Therefore, the crystallization of the crystallizable blocks overwrites the pre-existing mesophase morphology of the block

* Corresponding author. Tel.: +1-330-972-6931; fax: +1-330-972-8626.
E-mail address: cheng@polymer.uakron.edu (S.Z.D. Cheng).

0032-3861/01/$ - see front matter © 2001 Published by Elsevier Science Ltd.
PII: S0032-3861(01)00394-9

copolymer in the melt, resulting in an alternating crystalline and amorphous lamellar morphology [15,20–26]. For the confined crystallization in ordered phase morphologies, two cases have been identified. The first and obvious case is $T_{ODT} \gg T_g^a > T_c^c$ [1,2,4–10,16,26]. The crystallization of the crystallizable blocks is eventually confined within the pre-existing phase morphologies by the glassy amorphous phase and therefore, it is a so-called hard confinement. The second and less obvious case is $T_{ODT} \gg T_c^c \gtrsim T_g^a$ [3,11–15,17]. Although the T_g^a of the amorphous blocks is lower than the T_c^c of the crystallizable blocks, confined crystallization may still take place due to a relatively fast crystallization rate and a low molecular mobility of the block copolymers in the pre-existing phase (strong microphase separation). Thus, this is a so-called soft confinement.

However, detailed studies on how to quantitatively determine the boundary between unconfined and confined crystallization, and what is the difference between hard and soft confined crystallizations in crystalline–amorphous diblock copolymers have not been systematically reported. In this publication, efforts have been made to explore the difference between hard and soft confined crystallizations. A lamellae-forming poly(ethylene oxide)-*b*-polystyrene (PEO-*b*-PS, further abbreviated as EOS) diblock copolymer is purposely blended with a lower molecular weight (MW) PS homopolymer and a PS oligomer (PSO), respectively. Hence, the PS homopolymer and PSO are preferentially dissolved in the PS-block microdomains of the EOS sample [27]. It is controlled that these two blends possess an identical volume fraction of the PEO blocks, namely, 32 vol% This PEO volume fraction eventually leads to the formation of hexagonal PEO cylinders in the PS matrices for both blends. Since the PS matrices in these two blends are composed of PS with different MWs, the T_{ODT} of the blends and the T_g of the PS matrices (T_g^{PS}) have been observed to be different. Confined crystallizations of the PEO blocks within the cylinders of both blends are observed for the crystallization temperature of the PEO blocks (T_c^{PEO}) below 30°C. By controlling the MW of blending PS homopolymers, we are able to design blends following the relationships of (1) $T_{ODT} \gg T_g^{PS} > T_c^{PEO}$, which corresponds to a hard confinement for the PEO-block crystallization; and (2) $T_{ODT} > T_c^{PEO} \gtrsim T_g^{PS}$, which provides a soft confinement for the PEO-block crystallization. Different crystallization kinetics between the hard and soft confined crystallizations have been clearly identified.

2. Experimental

2.1. Materials and sample preparation

Synthesis of the lamellae-forming PEO-*b*-PS (EOS) diblock copolymer having $M_n^{PEO} = 8700\ g\ mol^{-1}$ and $M_n^{PS} = 9200\ g\ mol^{-1}$ has been reported previously [9]. EOS is blended with a PS homopolymer ($M_n^{PS} = 4600\ g\ mol^{-1}$) and a PS oligomer ($M_n^{PS} = 450\ g\ mol^{-1}$), to form two miscible polymer blends, abbreviated as EOS/PS-32 and EOS/PSO-32, respectively. The characterization data for PS homopolymer, PS oligomer, EOS, and EOS/PS-32 and EOS/PSO-32 blends are listed in Table 1.

In order to ensure the consistency of the phase behavior, uniform sample preparation procedure and thermal history were necessary. The samples were cast from a 5% (w/v) toluene solution, and the solvent was allowed to evaporate slowly under a dry nitrogen atmosphere at 50°C to prevent the crystallization of the PEO blocks. Residual solvent was further removed under vacuum at 50°C for one day, and the samples were then annealed at 95°C for 12 h for the EOS/PS-32 and at 65°C for the EOS/PSO-32 (because of its T_{ODT} being only 84°C). The samples were studied using different experimental techniques, including transmission electron microscopy (TEM), time-resolved simultaneous synchrotron small angle X-ray scattering (SAXS) and wide angle X-ray scattering (WAXS), and differential scanning calorimetry (DSC).

2.2. Equipment and experiments

Time-resolved, simultaneous one-dimensional (1D) SAXS and WAXS experiments were conducted at the synchrotron X-ray beamline X27C of the National Synchrotron Light Source in the Brookhaven National Laboratory. Two European Molecular Biology Laboratory (EMBL) 1D position sensitive detectors (PSD) were used to record

Table 1
The characterization data for PS homopolymer, PS oligomer, EOS, EOS/PS-32, and EOS/PSO-32

Samples	M_n (g mol^{-1})[a]	M_w/M_n[a]	f_{EO}	T_g^{PS} begin (°C)[c]	T_g^{PS} (°C)[c]	T_g^{PS} end (°C)[c]	T_m^{PEO} (°C)[c]	T_{ODT}(°C)[d]
PS homopolymer	4600	1.05	–	61	67	73	–	–
PS oligomer	450	1.18	–	− 26	− 21	− 15	–	–
EOS	17,900	1.05	0.47[b]	50	62	72	~ 51	160
EOS/PS-32	–	–	0.32	54	64	75	~ 50	175
EOS/PSO-32	–	–	0.32	7	16	22	~ 53	84

[a] Determined by SEC, using universal calibration.
[c] Determined by DSC.
[d] Determined by temperature-dependent 1D SAXS.
[b] Volume fraction of the PEO blocks determined by ^{1}H NMR.

SAXS and WAXS data, respectively. The zero pixel of the SAXS PSD was calibrated with a rat-tail, and the scattering vector q ($q = 4\pi \sin\theta/\lambda$, where the wavelength $\lambda = 0.1307$ nm and 2θ is the scattering angle) was calibrated with silver behenate. The WAXS PSD was calibrated using α-Al_2O_3. The sensitivity of both PSDs was calibrated using a ^{55}Fe source.

Isothermal crystallization measurements were carried out on a customized two-chamber hot stage that controlled the T_c^{PEO} to within ±0.1°C. The samples were preheated to 70°C in the melting chamber for 3 min, and then quenched (switched) to the second chamber with preset temperatures for isothermal crystallization. Both SAXS and WAXS data were recorded at different crystallization times (t_c). A heating rate of 1°C min^{-1} was used to study the melting behavior of the samples after complete crystallization of the blends. In order to detect the T_{ODT} of the sample, 1D SAXS experiments were conducted at a heating rate of 2°C min^{-1} under a dry nitrogen atmosphere. It was shown by combined thermogravimetric analysis and size exclusion chromatography (SEC) results that the blends possess stability up to 220°C when under an inert gas atmosphere for up to 3 h.

DSC experiments were carried out on a TA-2000 thermal analyzer to study isothermal crystallization and melting behavior of the EOS/PS-32 and EOS/PSO-32 blends. The DSC was calibrated with *p*-nitrotoluene, naphthalene, and indium standards. Isothermal crystallization was conducted by quenching the samples from the melt at 70°C to a preset T_c. The fully crystallized samples were then heated at a rate of 5°C min^{-1}. The endothermic peak temperature was taken as the melting temperature of the PEO crystals, T_m^{PEO}. The weight percentage crystallinity was calculated using an equilibrium heat of fusion for low MW PEO crystals (7.89 kJ mol^{-1}) [28], and was normalized to the PEO weight fraction in the blends. The crystal structure in both blends was identical with that of pure PEO, which is a monoclinic unit cell having $a = 0.805$ nm, $b = 1.304$ nm, $c = 1.948$ nm, and $\beta = 125.4°$. The space group is $P2_1/a$–C_{2h}^5 [29].

Transmission electron microscopy (TEM, JEOL 1200 EX II) experiments were carried out at an accelerating voltage of 120 kV. Thin slices were obtained using a Reichert Ultracut S (Leica) microtome on unoriented samples at −40°C. The sample was stained under RuO_4 vapor at room temperature for 20 min [30].

3. Results and discussion

3.1. The order–disorder transition and glass transition temperatures of both blends

The temperature parameter, T_{ODT}, can be obtained using temperature-dependent 1D SAXS experiments. The inset of Fig. 1a shows a set of SAXS results at different temperatures

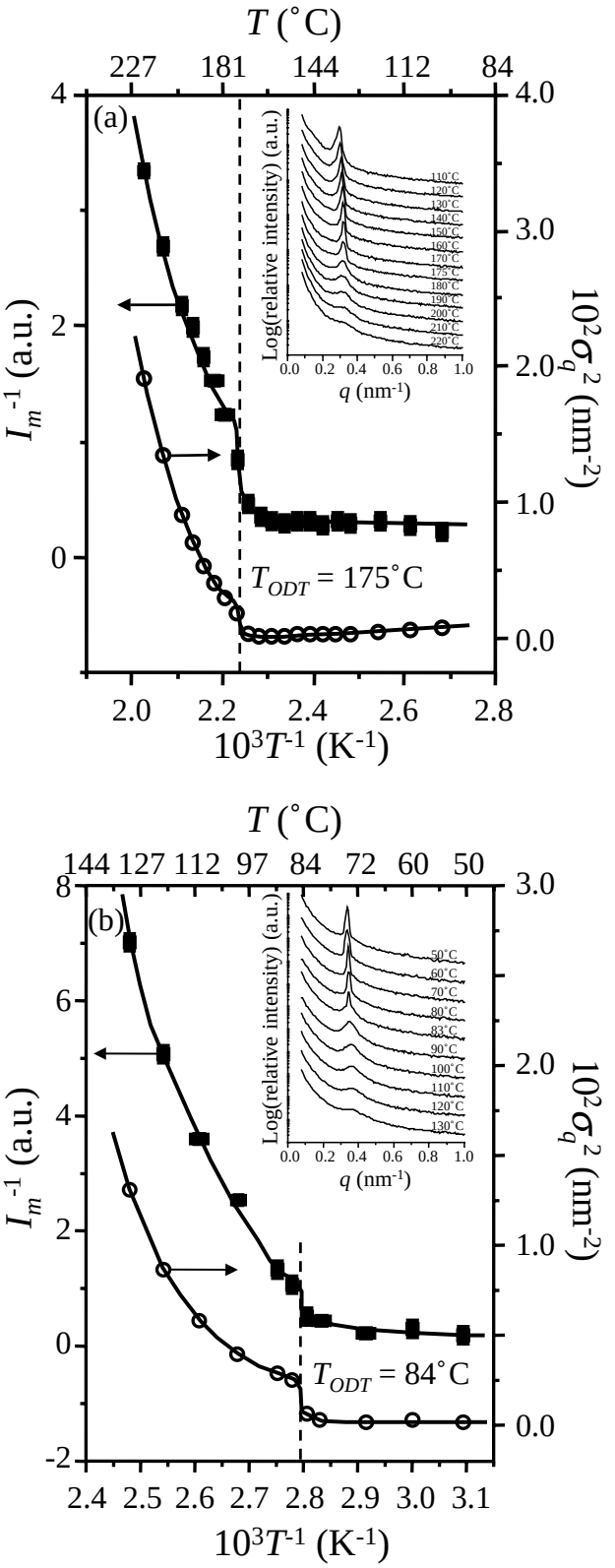

Fig. 1. (a) Relationships between the reciprocal SAXS scattering intensity (I_m^{-1}) and square of the half width at half height (σ_q^2) with respect to the reciprocal temperature (T^{-1}) for the EOS/PS-32 (a) and EOS/PSO-32 (b), respectively. The insets are sets of SAXS curves of the EOS/PS-32 and EOS/PSO-32 at different temperatures.

for the EOS/PS-32 blend. Below 175°C, there is a sharp first-order diffraction peak, indicating the microphase separated cylinder morphology (see below). There is a sudden change in both scattering peak intensity and the half-width at half-maximum around 175°C. Plots of the reciprocal scattering intensity (I_m^{-1}) and the square of the half-width at half-maximum of the scattering peak (σ_q^2) versus reciprocal temperature (T^{-1}) are shown in Fig. 1a. The temperature where the I_m^{-1} and σ_q^2 suddenly drop is defined as the T_{ODT}, as reported before [19,31]. Therefore, the T_{ODT} for the EOS/PS-32 is observed at 175°C. Similar results are shown in Fig. 1b for the EOS/PSO-32 blend, and the T_{ODT} for this blend is found at 84°C. Both T_{ODT} data are included in Table 1.

The T_g^{PS} is determined using DSC measurements. The DSC thermodiagrams for both EOS/PS-32 and EOS/PSO-32 are shown in Fig. 2a and b, respectively. It is evident that the T_g^{PS} for the EOS/PS-32 is 64°C while for EOS/PSO-32 it is 16°C. Both T_g^{PS}s are very close to the glass transition temperatures predicted by the Fox equation [32] based on different T_gs of the components in a miscible blend. With this calculation, the T_g of PS blends having MWs of 9200 and 4600 g mol^{-1} should be 64.3°C, while the T_g of PS blends having MWs of 9200 and 450 g mol^{-1} should be 16.8°C. Both results are very close to our experimental observations, and they further indicate that the PS homopolymer and PSO are only miscible with the PS blocks in the EOS. The T_g^{PS} data are also summarized in Table 1. Since the T_c^{PEO} in this study is between 10 and 30°C, it is clear that both blends serve our purpose to study the difference between hard and soft confined PEO crystallizations within nano-cylinders. Interestingly, in both blends the T_g^{PS} transition ranges are broader than that for the pure PS (see Table 1). This may be associated with the small size and the interfacial interactions in the microphase separated samples. Furthermore, the T_g^{PS} broadening is more evident in the case of the EOS/PS-32 than that of the EOS/PSO-32. Possible explanation may lie in different PS MW effects. Detailed understanding of this observation is under further investigation.

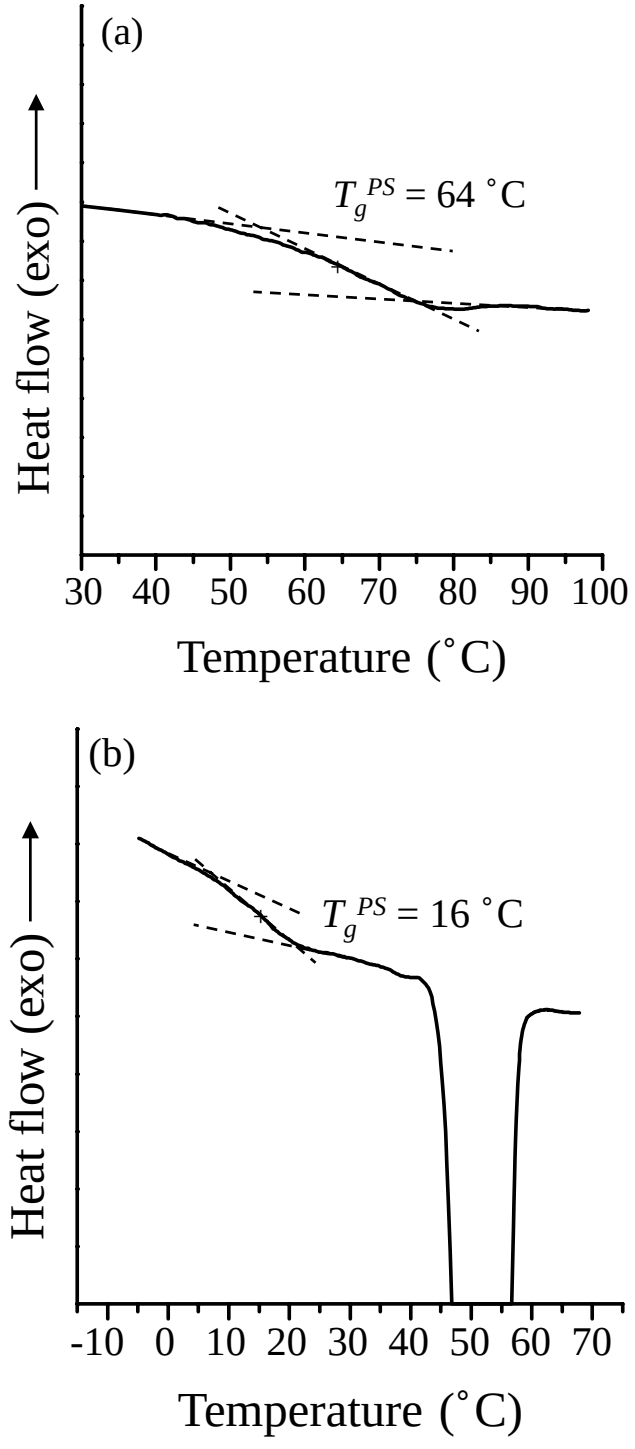

Fig. 2. DSC heating diagrams of EOS/PS-32 (a) and EOS/PSO-32 (b) at a rate of 5°C min^{-1}.

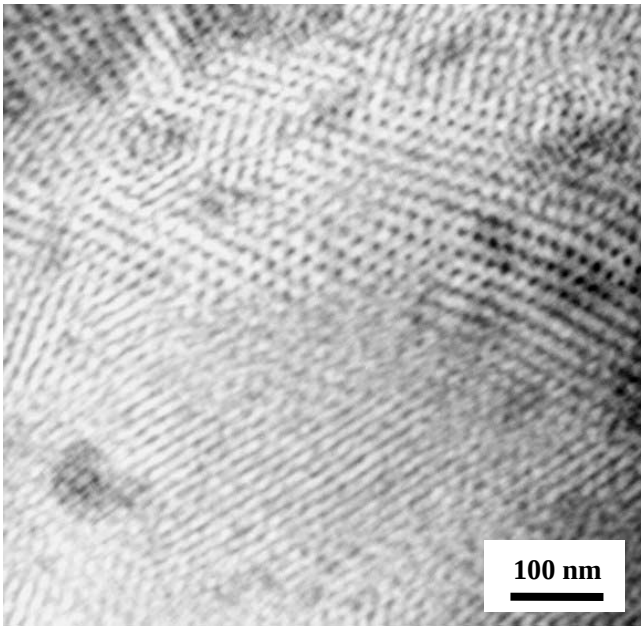

Fig. 3. Bright field TEM micrograph of the cylindrical phase morphology of an EOS/PS-32 thin slice stained by RuO_4.

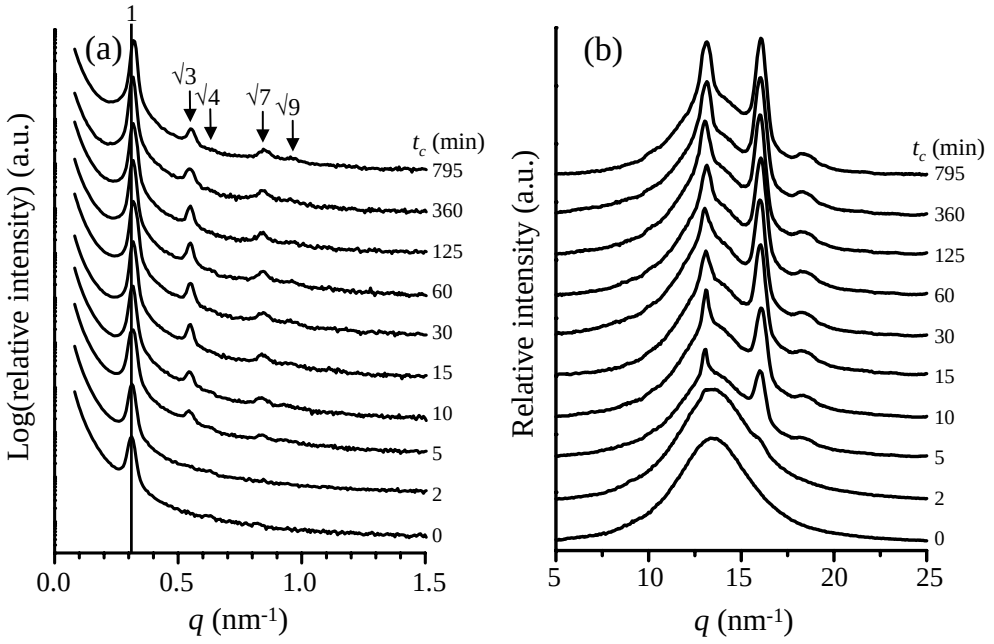

Fig. 4. Set of 1D SAXS (a) and WAXS (b) isothermal crystallization results for the EOS/PS-32 at $T_c^{PEO} = 25$°C.

3.2. Confined PEO crystallization in the EOS/PS-32 blend

After solution casting and annealing at 95°C for 12 h, the EOS/PS-32 blend appears transparent, indicating that the EOS and the PS homopolymer form a miscible blend. Fig. 3 shows the TEM micrograph of a thin slice of the EOS/PS-32 blend after staining with RuO_4 at room temperature for 20 min. Cylinders of the PEO blocks appear darker as compared to the PS matrix, since PEO is more easily stained by RuO_4 than PS [9]. In the upper part of this micrograph, one can observe that the PEO cylinders are packed into a hexagonal lattice (the head-on view), while in the lower part the cylinder orientation is tilted towards the side view. From the TEM, SAXS results, and the volume fraction of PEO blocks, the distance between neighboring cylinders is calculated to be 23.1 nm, and the diameter of the PEO cylinders is 13.7 nm.

As shown in Fig. 2a and Table 1, the T_g^{PS} of this blend is

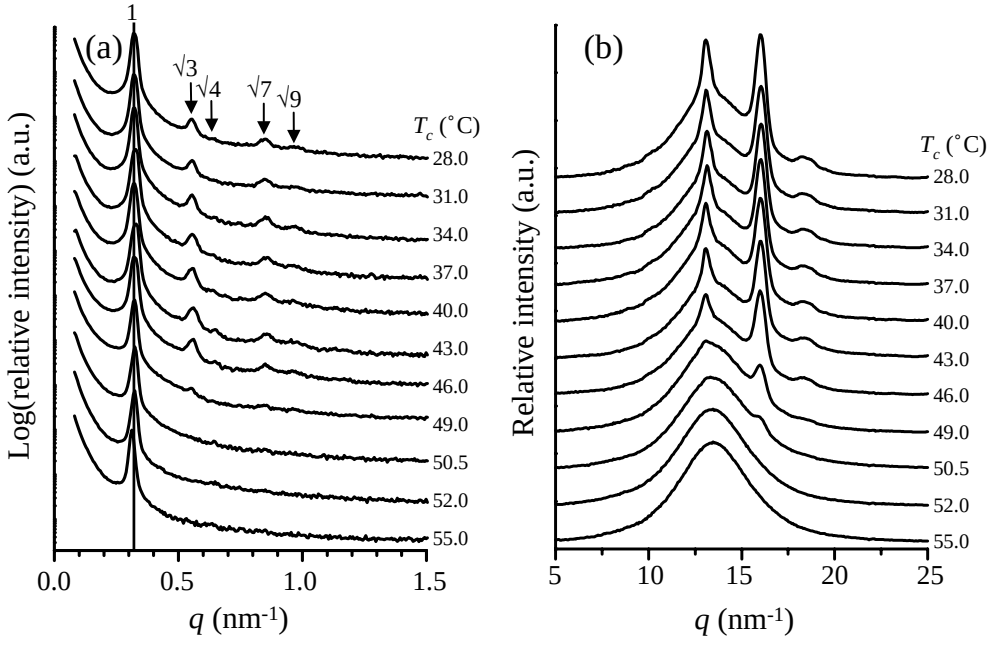

Fig. 5. Set of 1D SAXS (a) and WAXS (b) results during heating for EOS/PS-32 at 1°C min^{-1} to monitor the crystal melting after the sample was fully crystallized at 25°C.

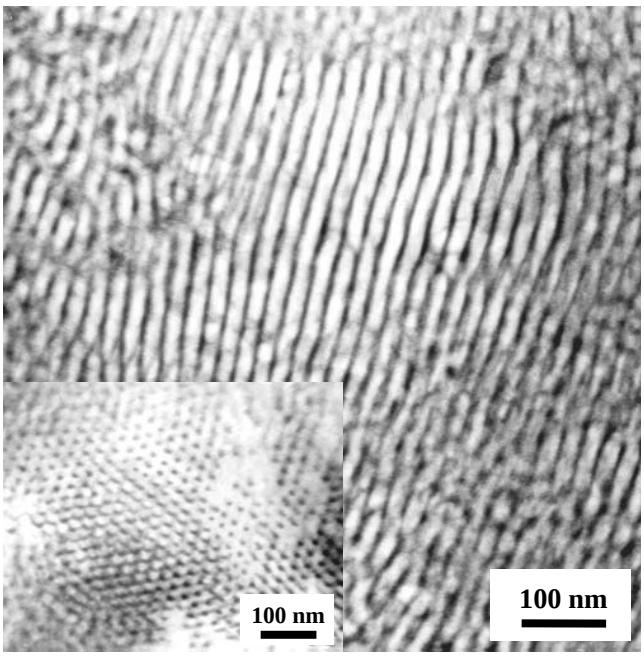

Fig. 6. Bright field TEM micrographs of the cylindrical phase morphology of an EOS/PSO-32 thin slice stained by RuO_4. The micrograph is a side view and the inset is a head-on view.

64°C, and is higher than the T_m^{PEO} (~50°C). Moreover, the T_{ODT} (175°C) is much higher than both T_g^{PS} and T_m^{PEO} in the EOS/PS-32 blend, indicating that the PEO and PS blocks are strongly segregated from each other. Therefore, the crystallization of the PEO blocks is confined within a hard PS matrix. Fig. 4a and b show time-resolved simultaneous 1D SAXS and WAXS results as the blend is isothermally crystallized at 25°C. In the initial stage (within $t_c = 2$ min) the SAXS pattern shows a sharp scattering peak, originating from the ordered hexagonal cylinders in the melt, and the WAXS pattern shows an amorphous halo at $q \sim 13.4\ nm^{-1}$ arising from both the non-crystalline PEO and PS blocks. With increasing t_c, the intensity of the first-order scattering peak in the SAXS increases. Higher orders of the scattering peak gradually appear and increase their intensities with t_c, due to a further enhancement of the electron density difference between the cylinders and the matrix [9]. Strong Bragg WAXS peaks at $q = 13.6$ and $16.5\ nm^{-1}$, which result from the PEO-block crystals, also gradually develop with increasing t_c. Since the first-order scattering peak remains almost at the same q value and the ordered cylindrical structure ($q/q^* = 1 : \sqrt{3} : \sqrt{4} : \sqrt{7} : \sqrt{9}$) is not changed throughout the crystallization, it is concluded that the PEO blocks crystallize in nano-cylinders confined by the glassy PS matrix.

Fig. 5a and b is a set of SAXS and WAXS results for the melting behavior of the EOS/PS-32 blend at a heating rate of 1°C min after the sample was fully crystallized at $T_c =$ 25°C. During heating, the SAXS scattering peaks start to decrease their intensity, while the WAXS Bragg reflections start to lower their intensities when the temperature approaches ~43°C. It is important to note that the positions of the multiple SAXS peaks remain at the same q values throughout the melting process. Therefore, the melting of the PEO-block crystals is also confined within the cylinders. These results reveal a clear concept of hard confinement effect for the PEO crystals in nano-cylinders.

3.3. Confined PEO crystallization in the EOS/PSO-32 blend

The EOS/PSO-32 blend also appears transparent after solution casting and annealing at 65°C for 12 h, indicating

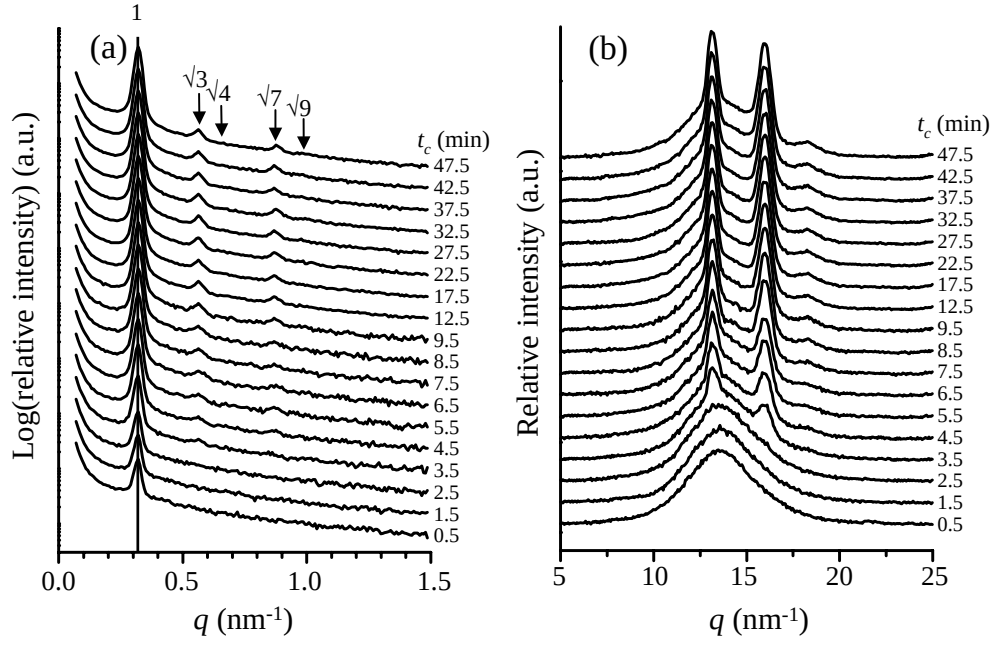

Fig. 7. Set of 1D SAXS (a) and WAXS (b) isothermal crystallization results for the EOS/PSO-32 at $T_c^{PEO} = 28$°C.

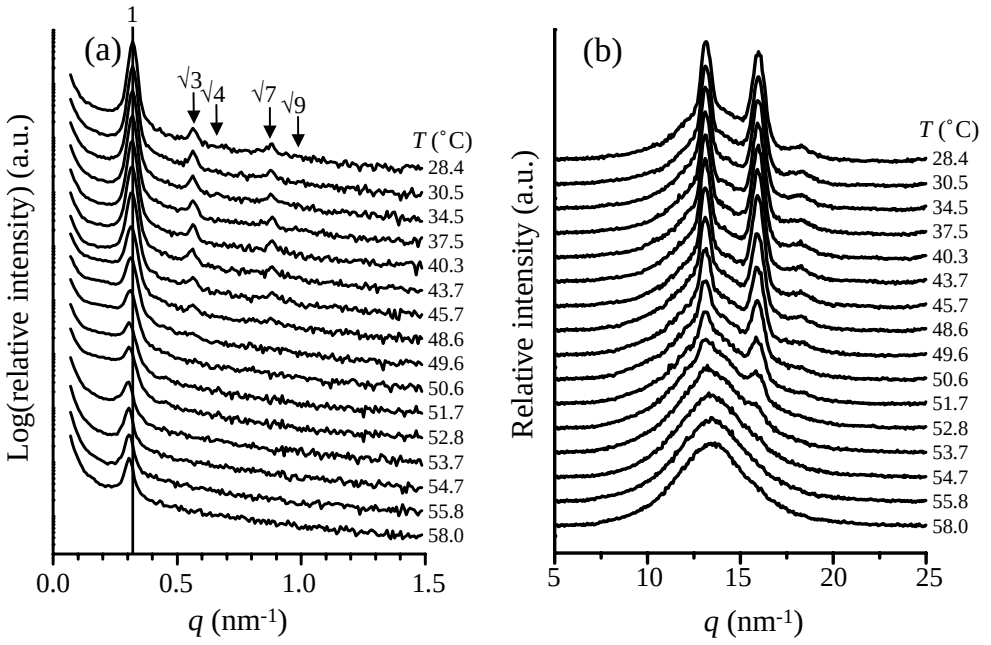

Fig. 8. Set of 1D SAXS (a) and WAXS (b) results for the EOS/PSO-32 at a heating rate of 1°C min^{-1} to monitor the crystal melting after the sample was completely crystallized at 28°C.

that the PSO is preferentially dissolved in the PS microdomains of the EOS. Fig. 6 shows the TEM micrograph of a thin slice of the EOS/PSO-32 blend stained by RuO_4 at room temperature. The side view of the PEO cylinders can be clearly observed. From the inset TEM micrograph, the PEO cylinders are packed into a hexagonal lattice (the head-on view). Since the volume fraction of PEO blocks in the EOS/PSO-32 blend is the same as in the EOS/PS-32 blend, the dimensions between neighboring cylinders and the diameter of the PEO cylinders are also 23.1 and 13.7 nm, respectively.

However, the T_{ODT} (84°C) of EOS/PSO-32 blend is much lower than that of EOS/PS-32 blend (175°C), and hence the PEO and PS phases are not as strongly segregated from each other as in the EOS/PS-32. Fig. 7a and b show time-resolved simultaneous 1D SAXS and WAXS results respectively, as the blend is isothermally crystallized at 28.0°C. In the initial stage (within $t_c = 2.5$ min) the SAXS patterns show a sharp scattering peak from the ordered cylinders in the melt, and the WAXS patterns possess an amorphous halo, again, arising from both non-crystalline PEO and PS blocks. With increasing t_c, the intensity of the first-order scattering peak in the SAXS increases. SAXS higher order scattering peaks gradually appear and their intensities also increase. At the same time, the PEO crystallization is evidenced by the development of the PEO crystal Bragg peaks in the WAXS patterns. The first-order SAXS scattering peak remains at the same q value and the ordered cylindrical structure ($q/q^* = 1 : \sqrt{3} : \sqrt{4} : \sqrt{7} : \sqrt{9}$) is kept throughout the crystallization. Although the T_c^{PEO}(28°C) is higher than the end of the T_g^{PS} (~22°C), the temperature difference does not seem large enough to destroy the confinement environment. Only when $T_c^{PEO} > 30$°C can a destruction of this soft confinement environment be observed [34], indicating that the PEO blocks crystallize in nano-cylinders surrounded by a soft PS matrix. Note that the T_c for the EOS/PSO-32 is higher than that for the EOS/PS-32, however, the PEO-block crystallization in the soft confinement environment in the EOS/PSO-32 is observed much faster than in the EOS/PS-32 in the hard confinement environment.

Fig. 8a and b is set of SAXS and WAXS results for the melting behavior of the EOS/PSO-32 blend at a heating rate of 1°C min^{-1}, after the sample was fully crystallized at $T_c =$ 28°C. Starting at ~45°C, the SAXS scattering peak intensity begins to decrease, and the WAXS Bragg reflections also gradually lower their intensities due to the initiation of the PEO crystal melting. Interestingly, different from the EOS/PS-32 blend, upon the onset of the PEO crystal melting (~45°C), the first-order SAXS scattering peak starts to slightly move towards lower q values, and the SAXS intensity at lower q values (between 0.16 and 0.3 nm^{-1}) substantially increases during further heating. These observations may be associated with the PEO crystal thickening process inside the cylinders in order to increase their thermodynamic stability. The PEO cylinder shape in the phase morphology may also start to change. After the PEO crystals completely melt, the hexagonal cylinder phase recovers. The destruction mechanism of the cylindrical phase morphology by the PEO crystal thickening needs further investigation.

3.4. Crystallization kinetics in hard and soft confinement environments

As shown in Sections 3.2 and 3.3, two different confinement

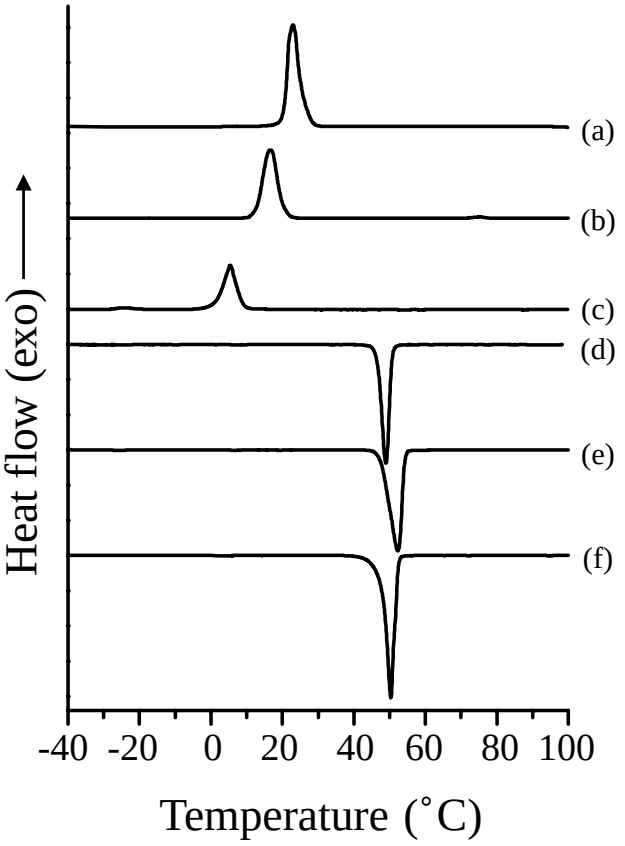

Fig. 9. Three sets of cooling and subsequent heating DSC diagrams for EOS (a for cooling and f for heating), EOS/PSO-32 (b for cooling and e for heating) and EOS/PS-32 (c for cooling and d for heating).

effects on the PEO crystallization and PEO crystal melting in both EOS/PS-32 and EOS/PSO-32 blends can be qualitatively identified. In order to further quantitatively understand the differences, crystallization kinetics for the PEO blocks in both blends are studied using DSC. Fig. 9 shows the cooling and subsequent heating DSC curves at 5°C min^{-1} for EOS, EOS/PS-32, and EOS/PSO-32, respectively. The non-isothermal exothermic and endothermic peak temperatures, T_c^{PEO}, T_m^{PEO}, and weight percentages PEO crystallinity obtained from Fig. 9 for the EOS, EOS/PS-32, and EOS/PSO-32 are listed in Table 2. As we can see for a first rough examination, the non-isothermal T_c^{PEO}s for both EOS/PS-32 and EOS/PSO-32 blends are lower than that for the lamellae-forming EOS sample. This may be attributed to the geometric confinement effect. A recent report [33] and our experimental findings [34] have shown that crystallization kinetics are substantially hampered as the nano-confinement geometry changes from a 1D confinement (lamellae) to a 2D confinement (cylinders), and finally to a 3D confinement (spheres). Comparing the overall weight percentage crystallinity in both blends (see Table 2), the crystallinity in the soft PS confinement in EOS/PSO-32 (75 wt%) is higher than that in the hard PS confinement in EOS/PS-32 (58 wt%). This clearly indicates the difference between these two confinements for the PEO-block crystallization.

Table 2
The nonisothermal peak T_c, T_m, and weight percent PEO crystallinity in EOS, EOS/PS-32, and EOS/PSO-32 (see Fig. 9)

Samples	Peak T_c (°C)	Peak T_m (°C)	Overall crystallinity (wt%)
EOS	22.9	50.3	61.0
EOS/PS-32	16.6	48.9	58.5
EOS/PSO-32	5.4	52.3	75.0

For a more quantitative investigation, the overall PEO crystallization rates for EOS/PS-32 and EOS/PSO-32 blends can be evaluated by the half-crystallization time ($t_{1/2}$), at which 50 wt% of the crystallinity is reached during an isothermal crystallization. Therefore, the faster the crystallization rate, the shorter the $t_{1/2}$. Fig. 10 shows the $t_{1/2}$ dependence upon the T_c^{PEO} for the EOS, EOS/PS-32, and EOS/PSO-32 samples. From this figure, the crystallization rate for EOS is much faster than those for both EOS/PS-32 and EOS/PSO-32 blends at the same T_c^{PEO}. This, again, indicates that the overall crystallization rate is depressed as the confinement morphology changes from 1D to 2D. However, the $t_{1/2}$ data for the EOS/PS-32 and EOS/PSO-32 blends also exhibit difference from each other. This difference must originate from different confined environments, i.e. hard versus soft confinements. As one can see, when the $T_c^{PEO} <$ 16°C (i.e. the T_g^{PS} of EOS/PSO-32 blend), the $t_{1/2}$ data for both the EOS/PS-32 and EOS/PSO-32 blends are quite similar. For $T_c^{PEO} > 16$°C, however, the $t_{1/2}$ for the EOS/PSO-32 blend becomes shorter than that for the EOS/PS-32 sample. With increasing T_c^{PEO}, the $t_{1/2}$ difference between these two blends becomes continuously enhanced. In particular, at

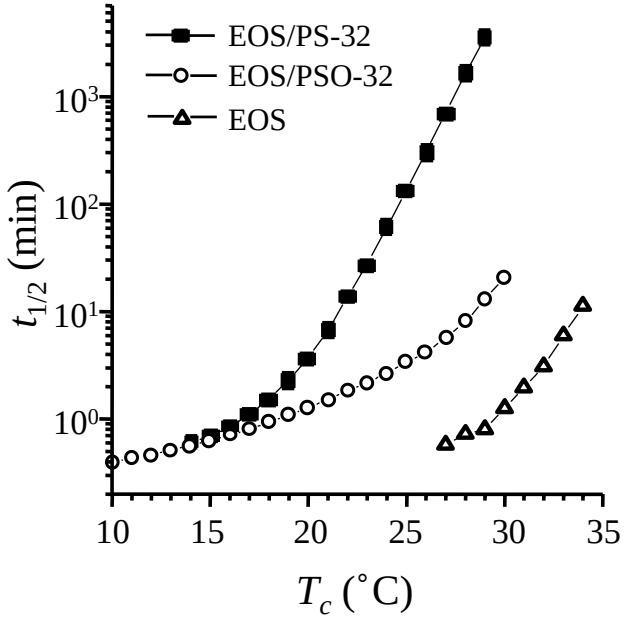

Fig. 10. The half-crystallization time ($t_{1/2}$) for both EOS/PS-32 and EOS/PSO-32. The data of pure PEO-*b*-PS is also included for comparison.

high T_c^{PEO}s, this difference is even larger than that between the EOS/PSO-32 blend and EOS. This reflects that the confinement effect on the PEO crystallization in the EOS/PSO-32 blend is increasingly released with increasing T_c^{PEO} in the soft confinement environment.

In order to explain the faster crystallization rate for the EOS/PSO-32 than the EOS/PS-32, the Avrami plots for both EOS/PS-32 and EOS/PSO-32 blends are shown in Fig. 11a and b. As we can see, the early crystallization processes in both samples fit into the Avrami equation. From the intercepts and slopes of the curves in Fig. 11a and b, ln K and n values can be obtained. The ln K values for both blends are shown in Fig. 12. It can be found that the ln K values for both samples are close to each other (the difference is equal or less than one unit). Note that ln K includes many parameters such as n power of linear crystal growth rate, geometric factor of crystals, primary nucleation density, etc. It is difficult to make quantitative conclusions for the overall crystallization process without knowing the quantities of each individual parameter in ln K.

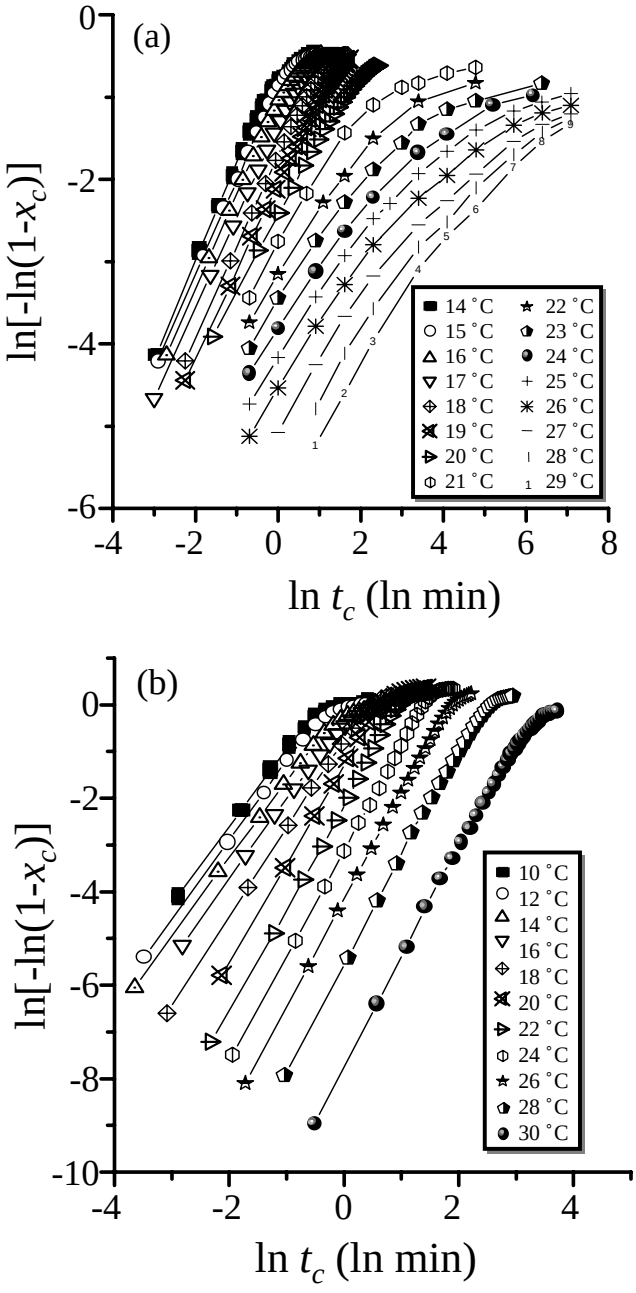

Fig. 11. The Avrami plots of the EOS/PS-32 (a) and EOS/PSO-32 (b) crystallized at different temperatures.

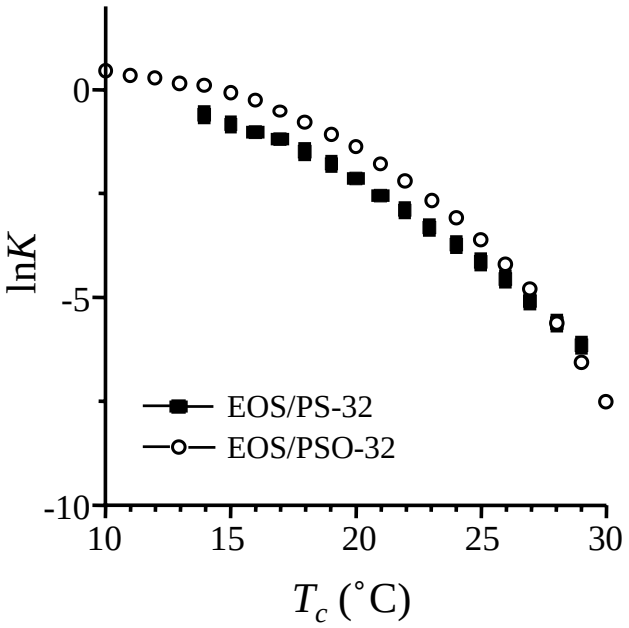

Fig. 12. Changes of the Avrami parameter, ln K, with respect to T_c^{PEO} in both blends.

The n values for EOS/PS-32 and EOS/PSO-32 blends are shown in Fig. 13. It can be observed that the n value of EOS/PSO-32 is always higher than that of EOS/PS-32 at the same T_c^{PEO} from 10 to 30°C. The n value for the EOS/PS-32 blend slightly decreases from ~1.2 at 14°C to ~0.8 at $T_c^{PEO} >$ 23°C. It is noted that for the hard confinement case in the EOS/PS-32 blend, the PEO crystal c-axis has been found perpendicular to the cylinder axis, and the crystal growth is along the cylinder axis direction in the T_c^{PEO} range in this study [35]. Moreover, a recent study reported that the crystals are inside the cylinders instead of locating at the interfaces [36]. Therefore, in the hard confinement of the PS matrix, the crystal growth dimension is more or less 1D in the cylinders, and the n value is thus around 1.0 when an athermal nucleation is assumed.

When the T_c^{PEO} increases above the T_g^{PS} of the EOS/PSO-32 blend, the n value for the EOS/PSO-32 gradually increases from ~1.6 at 16°C to ~2.0 at 23°C. The n value keeps around 2.1 between 23 and 30°C. Note that 23°C is almost identical to the end of the T_g^{PS} of the EOS/PSO-32 blend. Therefore, the PS matrix completely devitrifies above T_c = 23°C. Since the n value is related to the crystal growth dimensions, the increase in the n values from 1.6 to 2.0 for

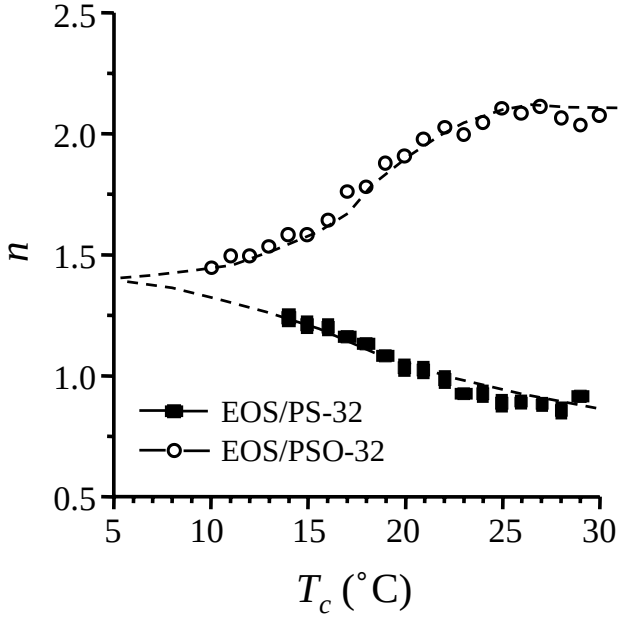

Fig. 13. Changes of the Avrami exponent, n, with respect to T_c^{PEO} in both blends.

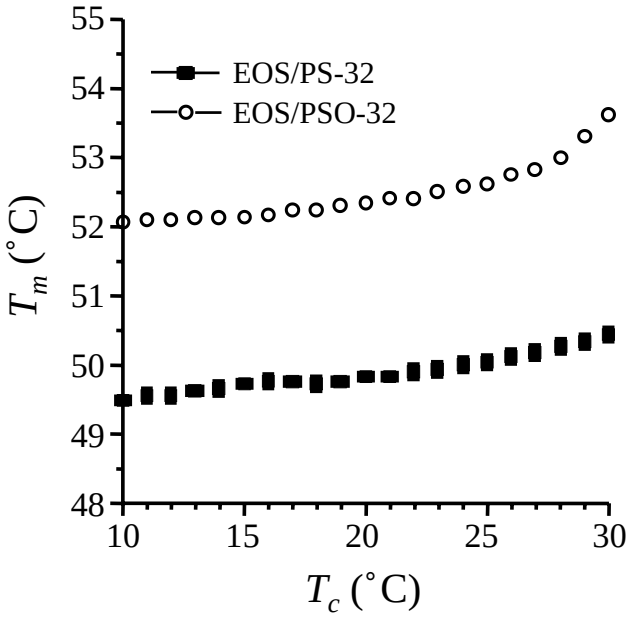

Fig. 14. Changes of the T_m of the PEO-block crystals in both blends with respect to T_c.

the EOS/PSO-32 may indicate an increase in the crystal growth dimension due to a gradual release of the soft confinement of the PS matrix. It is speculated that the PEO crystals in the soft confinement environment may distort the cylindrical confinement to reach a higher thermodynamic stability with increasing T_c. Note that this slight distortion may occur without change the gravity center of the cylinders, and thus does not affect the hexagonal packing in the phase morphology as observed in the SAXS results in Fig. 7a.

Based on previous discussion, the difference between hard and soft confinement effects can be mainly attributed to the difference in the crystal growth dimensions (the n values) in different samples. However, the fact that the $t_{1/2}$ and n values for both of the blends are very different while the ln K are close to each other may indicate that there must be changes in both the linear crystal growth rate and nucleation densities (or nucleation rate) at the same time in order to keep similar ln K in these two samples. This again needs further investigation.

In order to further prove that the thermodynamic stability of the PEO crystals in the soft confinement environment is higher than in the hard confinement environment, we plot the T_m^{PEO} obtained at different T_c^{PEO}s for both EOS/PS-32 and EOS/PSO-32 blends in Fig. 14. It is evident that the T_m^{PEO} of the PEO crystals in the soft confinement environment (EOS/PSO-32) is always 2.5°C higher than that in the hard confinement environment (EOS/PS-32). The crystallinity comparison for the EOS/PS-32 and EOS/PSO-32 in Fig. 15 also shows that the crystallinity of the PEO crystals in the soft confinement environment (EOS/PSO-32) is always ~25 wt% higher than that in the hard confinement environment (EOS/PS-32) in the T_c^{PEO} range studied. The higher T_m^{PEO} and crystallinity in the soft confinement environment clearly indicate that the thermodynamic stability of the crystals is higher than that in the hard confinement environment. This is because the soft confinement environment can be partially distorted during the PEO-block crystallization, while in the hard confinement environment the PEO-block crystals are exclusively constrained inside the cylinders surrounded by glassy PS matrix.

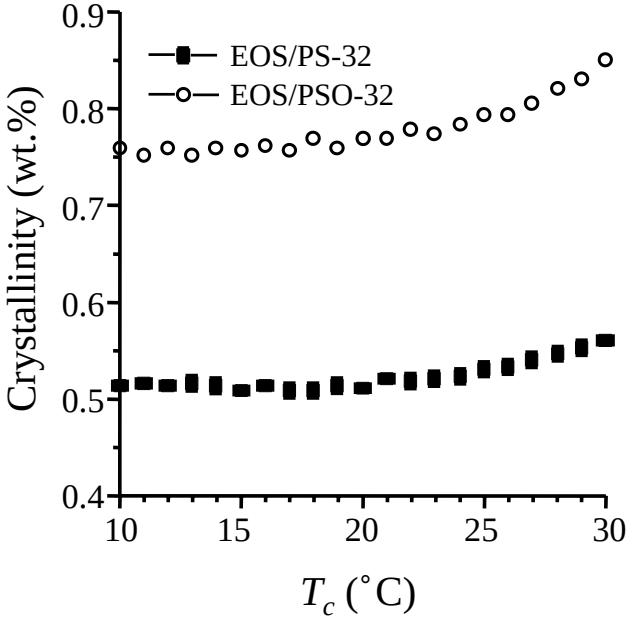

Fig. 15. Changes of the crystallinity of the PEO-block crystals in both blends with respect to T_c.

4. Conclusion

In summary, we controlled the MWs of PS in the EOS/PS blends to adjust the T_{ODT} and T_g^{PS}, and therefore created different nano-confinement environments for the crystallization of PEO blocks with an identical cylinder microphase morphology. Two cases of confinements have been observed: (1) hard confinement can be constructed when three temperature parameters fit to the relationship of $T_{ODT} \gg T_g^{PS} > T_c^{PEO}$; (2) soft confinement follows the relationship of $T_{ODT} > T_c^{PEO} \gtrsim T_g^{PS}$. It is particularly interesting that when the T_c^{PEO} is lower than the T_g^{PS} in the EOS/PSO-32 (16°C), its crystallization kinetics are nearly identical with that in the EOS/PS-32, indicating that a hard confinement for the EOS/PSO-32 has been reached. It has been found that crystallization kinetics for the EOS/PS-32 and EOS/PSO-32 blends above the T_g^{PS} of EOS/PSO-32 (16°C) are different, and at a constant T_c^{PEO} the PEO blocks in hard-confined cylinders crystallize much slower than those in the soft-confined ones. Crystallization kinetics studies by DSC show that the crystal growth dimension in the soft confinement environment is higher than that in the hard confinement environments. This leads to a higher thermodynamic stability of the crystals formed under the soft-confined environment compared to that of the crystals in the hard-confined environment.

Acknowledgements

This work was supported by the NSF (DMR-9617030). The time-resolved SAXS and WAXS research was carried out in part at the National Synchrotron Light Source in Brookhaven National Laboratory supported by the Department of Energy (DOE).

References

[1] Douzinas KC, Cohen RE. Macromolecules 1992;25:5030.
[2] Cohen RE, Bellare A, Drzewinski MA. Macromolecules 1994;27:2321.
[3] Kofinas P, Cohen RE. Macromolecules 1994;27:3002.
[4] Liu LZ, Yeh F, Chu B. Macromolecules 1996;29:5336.
[5] Hamley IW, Fairclough JPA, Terrill NJ, Ryan AJ, Lipic PM, Bates FS, Towns-Andrews E. Macromolecules 1996;29:8835.
[6] Hamley IW, Fairclough JPA, Ryan AJ, Bates FS, Towns-Andrews E. Polymer 1996;37:4425.
[7] Weimann PA, Hajduk DA, Chu C, Chaffin KA, Brodil JC, Bates FS. J Polym Sci, Polym Phys Ed 1999;37:2053.
[8] Zhu L, Cheng SZD, Calhoun BH, Ge Q, Quirk RP, Thomas EL, Hsiao BS, Yeh F, Lotz B. J Am Chem Soc 2000;122:5957.
[9] Zhu L, Cheng SZD, Calhoun BH, Ge Q, Quirk RP, Thomas EL, Hsiao BS, Yeh F, Lotz B. Polymer 2001;42:5847.
[10] Zhu L, Calhoun BH, Ge Q, Quirk RP, Cheng SZD, Thomas EL, Hsiao BS, Yeh F, Liu L, Lotz B. Macromolecules 2001;34:1244.
[11] Séguéla R, Prud'homme J. Polymer 1989;30:1446.
[12] Quiram DJ, Register RA, Marchand GR. Macromolecules 1997;30:4551.
[13] Quiram DJ, Register RA, Marchand GR, Ryan AJ. Macromolecules 1997;30:8338.
[14] Quiram DJ, Register RA, Marchand GR, Adamson DH. Macromolecules 1998;31:4891.
[15] Rohadi A, Endo R, Tanimoto S, Sasaki S, Nojima S. Polym J 2000;32:602.
[16] Cohen RE, Cheng PL, Douzinas KC, Kofinas P, Berney CV. Macromolecules 1990;23:324.
[17] Loo YL, Register RA, Ryan AJ. Phys Rev Lett 2000;84:4120.
[18] Zhang Q, Remsen EE, Wooley KL. J Am Chem Soc 2000;122:3642.
[19] Zhu L, Chen Y, Zhang A, Calhoun BH, Chun M, Quirk RP, Cheng SZD, Hsiao BS, Yeh F, Hashimoto T. Phys Rev B 1999;60:10022.
[20] Nojima S, Kato K, Yamamoto S, Ashida T. Macromolecules 1992;25:2237.
[21] Ishikawa S, Ishizu K, Fukutomi T. Eur Polym J 1992;28:1219.
[22] Rangarajan P, Register RA, Fetters LJ, Bras W, Naylor S, Ryan AJ. Macromolecules 1995;28:4932.
[23] Ryan AJ, Hamley IW, Bras W, Bates FS. Macromolecules 1995;28:3860.
[24] Ryan AJ, Fairclough JPA, Hamley IW, Mai SM, Booth C. Macromolecules 1997;30:1723.
[25] Mai SM, Fairclough JPA, Viras K, Gorry PA, Hamley IW, Ryan AJ, Booth C. Macromolecules 1997;30:8392.
[26] Hamley IW, Fairclough JPA, Bates FS, Ryan AJ. Polymer 1998;39:1429.
[27] Jiang M, Xie HK. Prog Polym Sci 1991;16:977.
[28] Cheng SZD, Wunderlich B. J Polym Sci, Polym Phys Ed 1986;24:577.
[29] Takahashi Y, Tadokoro H. Macromolecules 1973;6:72.
[30] Trent JS, Scheinbeim JI, Couchman PR. Macromolecules 1983;16:589.
[31] Sakamoto N, Hashimoto T. Macromolecules 1995;28:6825.
[32] Fox TG. Bull Am Phys Soc 1956;1:123.
[33] Chen HL, Hsiao SC, Lin TL, Yamauchi K, Hasegawa H, Hashimoto T. Macromolecules 2001;34:671.
[34] Zhu L, Huang P, Calhoun BH, Ge Q, Quirk RP, Cheng SZD, Thomas EL, Hsiao BS, Yeh F, Liu L, Lotz B. In preparation.
[35] Huang P, Zhu L, Calhoun BH, Ge Q, Quirk RP, Cheng SZD, Thomas EL, Hsiao BS, Yeh F, Liu L, Lotz B. Macromolecules. In preparation.
[36] Loo YL, Register RA, Adamson DH. J Polym Sci, Part B: Polym Phys 2000;38:2564.